BOLETIN DE LA SOCIEDAD ESPAÑOLA DE
Cerámica y Vidrio
www.elsevier.es/bsecv

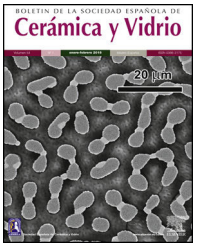

Enhancing bone tissue regeneration with rGO-coated Si-Ca-P bioceramic scaffold

Patricia Mazón[a,*], *Jeevithan Elango*[b], *José Eduardo Maté-Sánchez de Val*[b], *Piedad N. De Aza*[a]

[a] *Instituto de Bioingeniería, Universidad Miguel Hernández, Avda. Universidad s/n, Elche, 03202 Alicante, Spain*
[b] *Department of Biomaterials Engineering, Faculty of Health Sciences, UCAM-Universidad Católica San Antonio de Murcia, Guadalupe, 30107 Murcia, Spain*

ARTICLE INFO

Article history:
Received 27 February 2023
Accepted 17 May 2023
Available online 1 June 2023

Keywords:
Bioceramic
Reduced graphene
Osteoconductivity

ABSTRACT

Ceramic-based bone graft substitutes have been extensively studied for bone tissue engineering, due to their biocompatibility and osteoconductivity. Additionally, several studies have shown how graphene and its derivatives, due to their unique properties, can strongly promote cell adhesion, by enhance cellular adherence, proliferation, and osteoblast differentiation, and how graphene-based materials can promote spontaneous osteoblastic differentiation. The aim of this study was the use of a calcium silicophosphate ceramic, previously prepared in our laboratory, that presents excellent in vitro bioactivity, optimizing its operation by rGO coating. After coating with rGO any significant differences were observed in diffraction peaks from starting calcium silicophosphate ceramic, and SEM analysis showed a rough and undulating surface that favored a high specific surface area for promoting cell adhesion, proliferation and differentiation of cells. It could be confirmed by in vitro cell cultured with ahMSCs, showing adhesion and growing for cells with interconnected filaments extending over the surface, covering it after 7 days.

Potenciación de la regeneración ósea a través de una biocerámica de Si-Ca-P recubierta con grafeno reducido

Palabras clave:
Biocerámica
Grafeno reducido
Osteoconductividad

RESUMEN

Los sustitutos cerámicos para injertos óseos han sido estudiados ampliamente en ingeniería de tejidos debido a su biocompatibilidad y osteoconductividad. Además, varios estudios han demostrado cómo el grafeno y sus derivados, por sus propiedades únicas, pueden favorecer activamente la adhesión celular al mejorar la adherencia celular, la proliferación y la diferenciación de osteoblastos, y cómo los biomateriales basados en grafeno pueden promover la diferenciación osteoblástica espontánea. El objetivo de este estudio fue el uso de una

* *Corresponding author.*
E-mail address: pmazon@umh.es (P. Mazón).
https://doi.org/10.1016/j.bsecv.2023.05.002

cerámica de silicofosfato de calcio, previamente preparada en nuestro laboratorio, que presenta excelente bioactividad *in vitro*, optimizando su funcionamiento por recubrimiento con grafeno reducido. Tras el recubrimiento con rGO no se observaron diferencias significativas en los picos de difracción de la cerámica de silicofosfato de calcio de partida, y el análisis SEM mostró una superficie rugosa y ondulada que favorecía una superficie específica alta para promover la adhesión celular, la proliferación y la diferenciación de las células. Este hecho fue confirmado mediante cultivo celular *in vitro* con ahMSCs, observándose adhesión y crecimiento de células con filamentos interconectados que se extendían sobre la superficie, cubriéndola completamente tras 7 días.

Introduction

Biomaterials demand has been growing exponentially in the last few decades. Trauma injuries and increasing life expectancy mainly, have focused many attention on designing and implementing scaffolds for bone tissue repair and bone replacement. Bone tissue, once damaged or necrotic, does not possess sufficient regeneration ability in order to undergo self-repair, because of nonvascular and cell-free characteristics. Suitable scaffold materials could be implemented to accelerate the growth and differentiation of bone cells [1]. In the last decades, there is a great variety of synthetic materials that are developed as scaffolds, such as synthetic polymers, ceramics, and metals. However, their ability to repair bone tissue continues being less than that of autologous bone grafts and allogenic bone grafts do it. Nevertheless, availability for autologous ones, and immunogenic response for allogenic ones are problematic. In another hand, synthetic scaffolds presented disadvantages as compatibility, toxicity, anticoagulant properties, lack of adequate mechanical properties, etc.

Ceramic-based bone graft substitutes such as hydroxyapatite (HA), β-tricalcium phosphate (β-TCP), and bioactive glasses have been widely studied for bone tissue engineering, particularly for bone repair, due to their biocompatibility and osteoconductivity [2]. Also, the incorporation of ions as Si, Mg, or Zn into their chemical compositions could improve stem cells proliferation when they are seeded on the materials, and their differentiation into osteoblastic cells [3].

Graphene and its derivatives possess remarkable properties that are currently being extensively researched in various fields, including gene therapy, bioelectronics, and tissue engineering. These materials have a large surface area, high strength and flexibility, and the ability to adapt to irregular surfaces, as well as exceptional thermal and electrical conductivity and optical properties. The aromatic structure's planar carbon–carbon bonds generate free π electrons and reactive sites, which make surface functionalization a straightforward process [4,5]. Moreover, they have demonstrated the ability to induce stem cells to differentiate into specific tissue cells and regulate cell interactions.

Mechanical properties of bioceramics in bone tissue engineering could be improved by combination with graphene derivatives, without hampering their structures or biocompatibilities [6]. Furthermore, several studies have shown how graphene and its derivatives can strongly promote cell adhesion [7], by enhance cellular adherence, proliferation, and osteoblast differentiation [8], and how the high elastic modulus of graphene-based materials can promote spontaneous osteoblastic differentiation [9].

Reduced graphene oxide (rGO) is a derivative of graphene obtained through chemical or thermal reduction of graphene oxide (GO). rGO is characterized by having a lower number of oxygenated groups, which enables the creation of defects in the atomic structure that favor interaction with biomolecules, cells and polymers [10]. Because of that, rGO combined a structural similarity to pristine graphene (high surface area and strength) [11,12], and on the contrary to GO, presents highly conductivity [13] and moderate dispersibility in water [14,15]. However, there are still oxygen functional groups in rGO for functionalization, and the amount of that could be controlled via different reduction techniques.

Previously, we reported that mesenquimal stem cells (MSCs) isolated from adult human bone marrow (ahMSCs) were able to successfully grow and adhere on TCP, Si-TCP and Si-Ca-P ceramics [16–18]. This study aimed to enhance the functionality of a bioceramic scaffold composed of Si-Ca-P by optimizing its surface properties through the application of a thin layer of reduced graphene oxide (rGO). The goal was to achieve complete coverage of the scaffold with a uniform layer of rGO, in order to improve its biocompatibility and promote the growth and differentiation of stem cells. Also, we determined its in vitro osteogenic potential, in order to know the mechanisms by which reduced graphene induces osteoblastic differentiation.

Materials

Synthesis and characterization of the ceramic as base material for the scaffold

The starting ceramic material, Nurse's A-phase ceramic (from now and beyond named as $SiCaP_2O_5$), was prepared through a solid-state reaction method from a stoichiometric mixture of calcium hydrogen phosphate anhydrous ($CaHPO_4$; Panreac S.L.U., Barcelona, Spain), calcium carbonate ($CaCO_3$ > 99.0 wt%; Fluka-Sigma Aldrich Quimica SL, Madrid, Spain) with an average particle size of 13.8 μm, and silicon oxide (SiO_2 > 99.7 wt%; Strem Chemicals UK Ltd, Cambridge,

UK) with an average particle size < 50 μm. Discs-shaped $SiCaP_2O_5$ samples, measuring 7 mm in diameter and 3 mm in thickness, were cut from the sintered bulk with a diamond saw. For more information on the technique and the ceramic's characterization, please refer to a previous publication [19].

The ground sample in this study was subjected to mineralogical characterization by X-ray Diffraction, XRD (Bruker-AXS D8 Advance, Karksruhe, Germany), using $CuK_{\alpha 1,2}$ radiation (1.54056 Å) and operating at 40 kV at 30 mA and compared with the data base provide by Joint Committee on Powered Diffraction Standards (JCPDS).

The material's microstructure was analyzed using Scanning Electron Microscopy, SEM (SEM-Hitachi S-3500N, Ibaraki, Japan) using an accelerating voltage of 20 kV. Chemical composition analysis was conducted by fitting the scanning electron microscope with an energy dispersive X-ray spectroscopy, EDS system (INCA system by Oxford Instrument Analytical, UK). Prior to SEM-EDS observations, the samples were coated with palladium.

The porosity and pore size distribution for $SiCaP_2O_5$ ceramic was analyzed by mercury porosimetry using a Poremaster-60 GT (Quantachrome Instrument, Boyton Beach, FL) within the pressure range of 5.395–410785 kPa, which corresponds to a pore diameter range between 300 and 0.0035 μm. Three samples were analyzed using this technique. An additional sample was used in each case if the obtained porosity values differed by more than 5%.

Reduced graphene coating of ceramic base material for scaffold

Reduced graphene coating of $SiCaP_2O_5$ ceramic preparation

To apply the GO coating to the $SiCaP_2O_5$ ceramic discs, the discs were immersed in 50 ml of aqueous GO suspensions (GRAPHENEA, San Sebastian, Spain) with a concentration of 0.5 mg/ml for five cycles of 10 min, followed by 10-min drying periods at 100 °C between each cycle. After this, the GO-$SiCaP_2O_5$ samples were dried overnight at 100 °C. Subsequently, the GO-$SiCaP_2O_5$ samples were immersed in an aqueous solution of ascorbic acid (20 mM) at 70 °C for 3 h, using the method proposed by Fernández-Merino et al. [20], to reduce the GO. The reduced graphene oxide-coated $SiCaP_2O_5$ (rGO-$SiCaP_2O_5$) scaffolds were washed with distilled H_2O and dried at 37 °C.

rGO-$SiCaP_2O_5$ scaffolds were individually packaged and sterilized by gas-plasma (Sterrad-1005TM, ASP Irvine, Ca.).

Characterization of reduced graphene coated-$SiCaP_2O_5$ scaffold

Mineralogical characterization of rGO-$SiCaP_2O_5$ scaffolds were evaluated from powder by XRD, following the same protocol described for ceramic starting material for uncoated samples, and results were compared with these ones. The surface morphology was characterized by SEM-EDS as described for uncoated material.

The chemical structure for coated sample was studied with X-ray photoelectron spectroscopy, XPS Spectroscopy (K-Alpha, Thermo-Scientific) from powder of the samples.

Porosity and pore size distribution of scaffold were analyzed, in the same way as starting ceramic, by mercury porosimetry for comparative purpose.

In vitro bioactivity of the reduced graphene coated-$SiCaP_2O_5$ scaffold

An in vitro bioactivity study was conducted to assess the calcium phosphate capability induction by immersing the scaffolds in an acellular simulated body fluid (SBF), according to the Standard ISO/FDIS 23317:2014 [21]. The scaffolds were positioned inside containers made of polystyrene and filled with 50 ml of SBF, which had an ion plasma concentration similar to that of human blood plasma at pH 7.40. Next, the containers with the SBF and samples were placed in a shaking water bath and incubated at 37 °C. After different periods of immersion, which ranged up to 14 days, the specimens were taken out, rinsed with deionized water, and air-dry at room temperature. In order to examine the surfaces of the specimens after being exposed to SBF, they were coated with palladium and subjected to surface analysis using SEM and microanalysis with EDS. At specific immersion intervals, the SBF was collected and its calcium, silicon, and phosphorus ion concentrations were analyzed using inductively coupled plasma optical emission spectrometry (ICP-OES PerkinElmer Optima 2000).

Finally, in order to know the chemical bond composition of the new precipitated layer, Fourier Transform Infrared Spectrometry with Attenuated Total Reflectance accessory, ATR–FTIR (Thermo Scientific Nicolet iS5 equipped with an iDR ATR accessory) was used.

Cell culture

In vitro cell culture

ahMSCs (ATCC PCS-500-012™) were purchased from LGC GmbH, Louis-Pasteur, Luckenwalde, Germany and were used to evaluate the biocompatibility of $SiCaP_2O_5$ and rGO-$SiCaP_2O_5$ scaffold. In brief, the cells were cultured as per the standard cell culture protocol using complete mesenchymal stem cells basal medium with the required supplements as per the LGC GmbH instruction. The cells with complete medium were cultured in a 5% CO_2 incubator at 37 °C until confluence, followed by sub-culture. The cells with passage n° 4–7 were used for the biocompatibility experiments. Every time, the cells were trypsinized using 0.25% trypsin/EDTA as they were adhered on top of the samples, and then quantified using an automated Invitrogen cell counter (Invitrogen, Carlsbad, CA, USA).

Cell proliferation

Before cell culture, samples were sterilized overnight under UV by using a UV Sterilizer, 9W, 60 Hz (SKU: OT-HSYXF-2624-EU, model YM-9002, China). The sterilized samples were transferred into 48 well culture plates and ahMSCs with a cell density of 5×10^4 were seeded on top of the samples. The cells without test samples were considered as control. The cells were allowed to grow for 7 days and then the total number of grown cells was counted by automated cell counter (Invit-

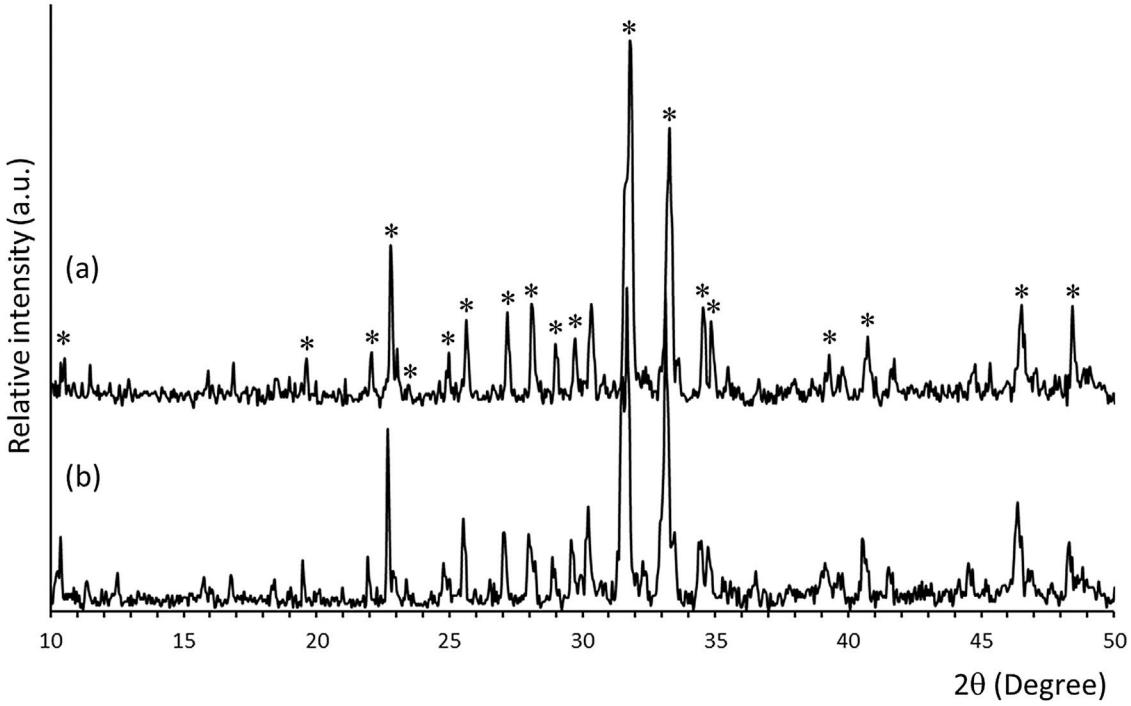

Fig. 1 – X-ray diffraction pattern from (a) $SiCaP_2O_5$ ceramic and (b) rGO-$SiCaP_2O_5$ scaffold.

rogen). The percentage of cells proliferation of tested samples was calculated by comparing control group.

Cell cytotoxicity

The cytotoxic effect of $SiCaP_2O_5$ ceramic and rGO-$SiCaP_2O_5$ scaffold were determined by MTT Assay Protocol as per our previous protocol [22]. In brief, the ahMSCs were seeded onto the top of the samples at a density of 5×10^4 cells in 48 well culture plates as described earlier, and the positive control cells were seeded without any sample. The ahMSCs with $SiCaP_2O_5$ and rGO-$SiCaP_2O_5$ were allowed to culture for 7 days before MTT treatment. 50 μl of MTT reagent with a concentration of 5 mg/ml phosphate buffer saline (PBS) was added in each well along with culture medium for 3 h. Then, the wells were gently washed with PBS twice and the formazan crystals were solubilized with DMSO at 37 °C, 5% CO_2 for 15 min. Then 100 μl of solubilized formazan crystals were transferred to a transparent-flat-bottom 96-well plate and the absorbance was recorded at 570 nm in a SpectraMAX Id3 plate reader.

Cell loading ability

In order to evaluate the total capacity of cells that can adhere on top of the $SiCaP_2O_5$ and rGO-$SiCaP_2O_5$ samples, we have done the cell loading ability as per our earlier protocol [22]. Briefly, the ahMSCs with a cell density of 1×10^5 were seeded on top of the samples as described earlier. After 6 h of cell seeding, the samples were transferred to new 48 well plate in order to quantify the exact cell number that have been attached on top of the samples. At the same time, the cells attached other than bioactive ceramic $SiCaP_2O_5$ samples in 48-well plates were also quantified for comparison.

Cell adhesion behavior on $SiCaP_2O_5$ by scanning electron microscopy

To investigate the cell adhesion behavior, the ahMSCs were seeded with a cell density of 5×10^4 on all the $SiCaP_2O_5$ and rGO-$SiCaP_2O_5$ samples and cultured for 3 and 7 days. After 7 days' culture, the cells were gently washed with PBS and were fixed with 2.5% glutaraldehyde for 1 d, followed by consecutive fixing with 4% paraformaldehyde for a day. The samples were briefly washed with PBS after each fixation, and the samples were dehydrated with increased ethanol concentration (serial dilutions) starting from 10, 25, 50, 75 and 100% ethanol (30 min. in each dehydration). After dehydration the samples were briefly air dried for the analysis by SEM.

Results

Mineralogical characterization by XRD of uncoated and coated samples ($SiCaP_2O_5$ and rGO-$SiCaP_2O_5$) is shown in Fig. 1. Each diffraction peak for starting ceramic (Fig. 1a) was identified as the characteristic reflection of Nurse's A phase (JCPDS card n° 11-0676) indicated on figure by an asterisk (*). A slight displacement from the corresponding JCPDS card, about 0.1°, was observed for diffraction peaks, due to solid solution. Any significant differences were observed for the reduced graphene coated sample by this method (Fig. 1b).

The XPS survey spectra (Fig. 2a) and the information included in Table 1 were use to describe elemental composition of $SiCaP_2O_5$ ceramic and rGO-$SiCaP_2O_5$ scaffold. Notable differences were found related with calcium, silicon and phosphorous small content in rGO-$SiCaP_2O_5$ scaffold, and as well in the biggest content in carbon that it presents.

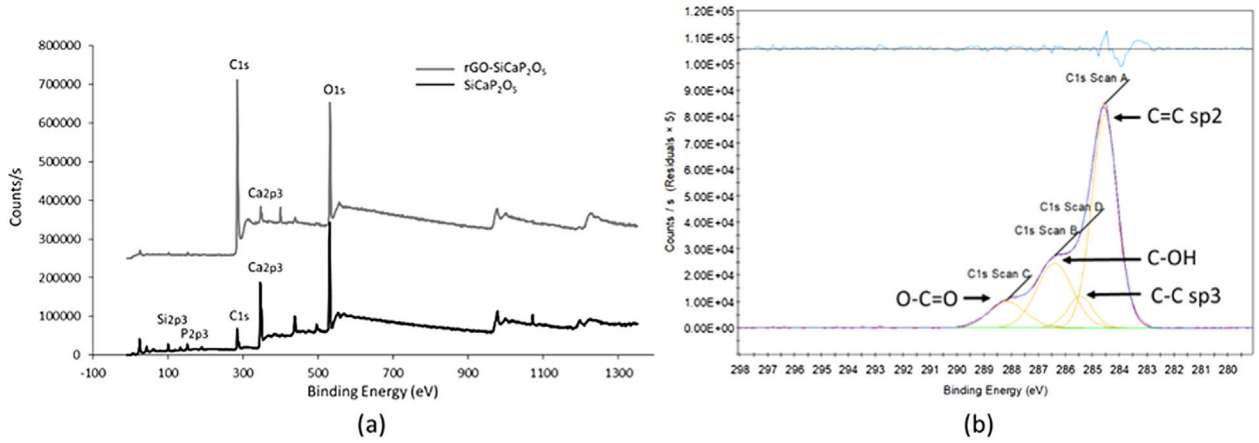

Fig. 2 – (a) XPS survey spectra of $SiCaP_2O_5$ (black line) and rGO-$SiCaP_2O_5$ (gray line), and (b) C1s spectra of rGO-$SiCaP_2O_5$ and its deconvolution.

Table 1 – Atoms' percentage in the structure of $SiCaP_2O_5$ and rGO-$SiCaP_2O_5$ from XPS survey.

% Atoms	C1s	Ca2p3	Si2p3	P2p3
$SiCaP_2O_5$	48.12	35.3	12.3	4.29
rGO-$SiCaP_2O_5$	97.09	1.79	1.01	0.11

In the C1s XPS spectra (Fig. 2b), four distinct peaks can be discerned at 284.56 eV (C = C sp2), 286.40 eV (C—C sp3), 285.46 eV (C—OH) and 288.14 eV (O—C = C).

SEM was used to examine the microstructure of the rGO-$SiCaP_2O_5$ scaffold (Fig. 3). It could be clearly observed rGO-sheet covering the entire ceramic disk with a thickness about 2 μm, and a gap between both. For rGO sheet an irregular surface was observed, as it was expected, while the ceramic showed a granular microstructure.

Microporosity level and its distribution were studied by mercury porosimetry for $SiCaP_2O_5$ ceramic and rGO-$SiCaP_2O_5$ scaffold (Fig. 4). With increasing pressure, mercury infiltrated the progressively smaller pores. As expected no large difference was observed for both samples related to intra- and interparticle porosity. Summarized results for porosimetry analyzed are presented in Table 2 for a better comprehension.

In a previous study, in vitro bioactivity of $SiCaP_2O_5$ ceramic was investigated [23]. In order to determine changes in the bioactivity of the rGO-$SiCaP_2O_5$ scaffold, its bioactivity was assessed following immersion in SBF for different periods of time. Surface morphology was evaluated by SEM-EDS after each immersion interval. The results after soaking for 1, 5 and 7 days are shown in Fig. 5a–c. After 1 day soaking time in SBF, only rGO sheet morphology was observed with any evidence of bioactivity (Fig. 5a), while after 5 days (Fig. 5b) a small and disperse globular precipitate was observed over rGO sheet, that increased in sized covering the entire surface after 7 days (Fig. 5c). Precipitated layer was identified as hydroxyapatite (HA)-like by SEM-EDS microanalysis, with a Ca/P ratio on average ~2.6. This ratio, higher than the one HA stoichiometric presents, suggests a carbonate-hydroxyapatite (CHA) is growing on the surface of scaffold.

Once saturation on the surface of the scaffolds was confirmed, a longer experiment was conducted to analyze the precipitate layer in depth, with a maximum soaking time of 14 days. The precipitate layer was examined by SEM cross-section analysis, as shown in Fig. 5d. To determine the thickness of the precipitate on the scaffold, SEM measurements were taken by recording 20 measurements per sample in triplicate. The precipitate layer was continuous with a thickness value reaching 8.6 μm. A gap between the precipitated layer and reduced graphene sheet was observed due to vacuum use in SEM technique, additionally to the one between reduced graphene sheet and ceramic.

ICP-OES was used to analyze the changes in ion concentrations (calcium, phosphorus, and silicon) from the SBF over different immersion periods. These results are presented in

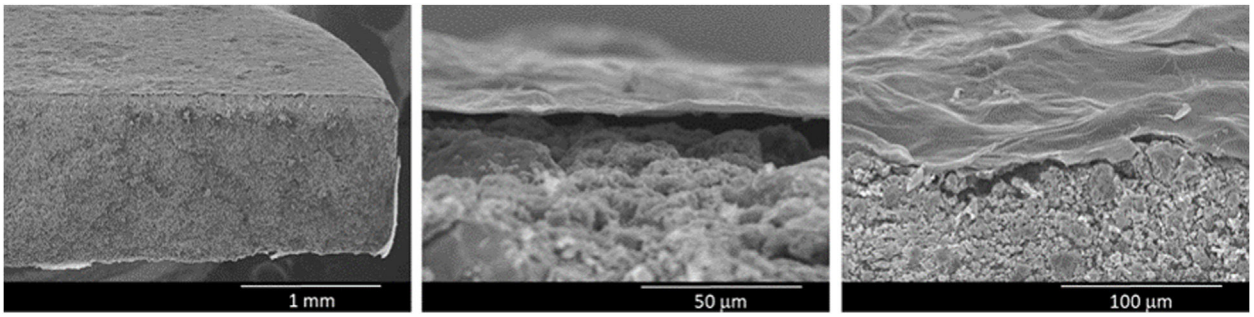

Fig. 3 – Scanning Electron Microscopy micrograph with different augmentations of rGO-$SiCaP_2O_5$ scaffold.

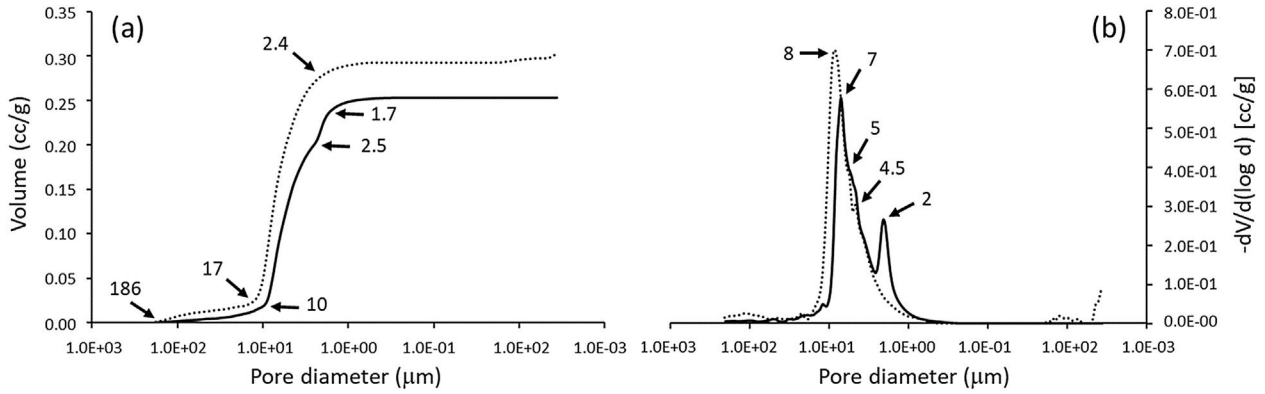

Fig. 4 – (a) Cumulative curve vs pore diameter and (b) differential volume for $SiCaP_2O_5$ ceramic (dotted line) and rGO-$SiCaP_2O_5$ scaffold (continuous line).

Table 2 – Porosity and density results for $SiCaP_2O_5$ ceramic and rGO-$SiCaP_2O_5$ scaffold.

	Apparent density (g/cc)	Total porosity (%)	Intrusion volume (cc)	Intraparticle porosity (%)[a]	Interparticle porosity (%)[b]	Theoretical porosity (%)
$SiCaP_2O_5$	1.5530	47.2147	0.1311	11.4397	35.7749	47.2092
rGO-$SiCaP_2O_5$	1.7738	43.9816	0.1251	16.4825	27.4992	43.9816

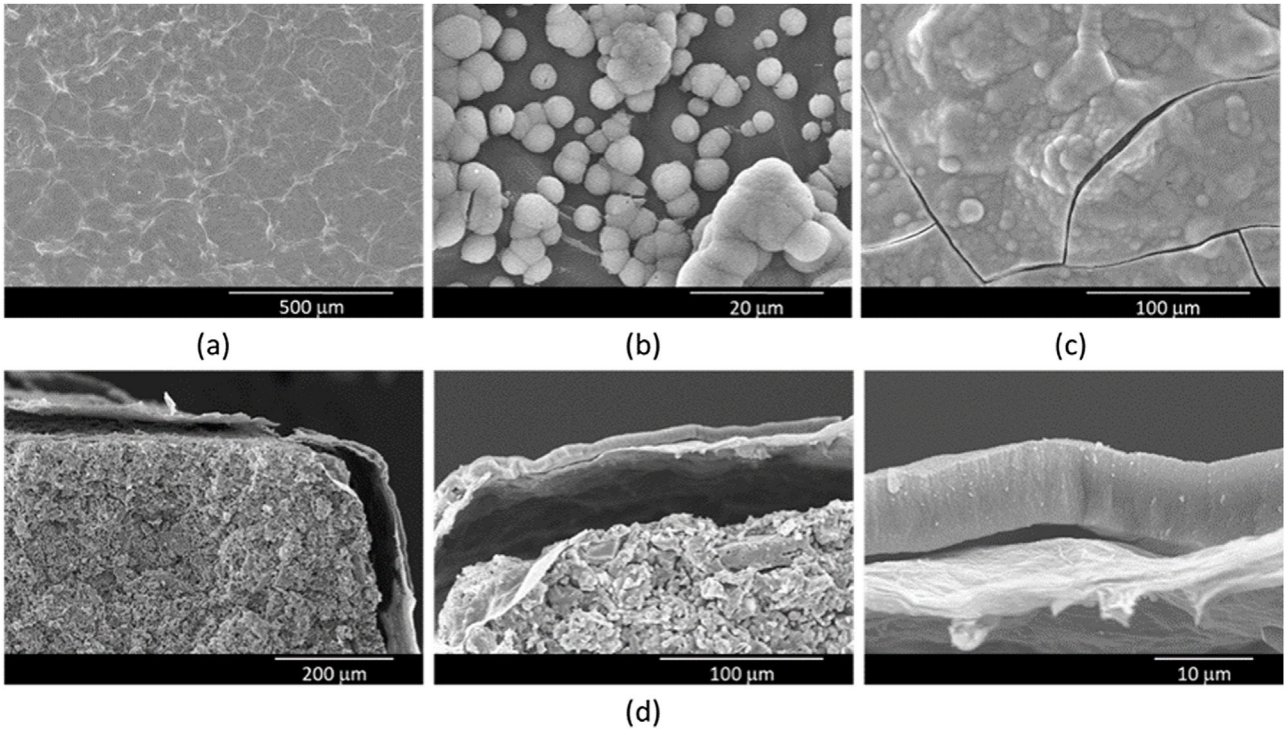

Fig. 5 – SEM images of the rGO-$SiCaP_2O_5$ scaffold's surface morphology after soaking time in SBF for (a) 1 day (b) 5 days, (c) 7 days, and (d) cross-section images, after soaking time in SBF for 14 days.

Fig. 6. Calcium concentration increased until day 5 of SBF soaking as the silicon one, which indicate an initial dissolution of the material previous to precipitate formation on the surface. As the HA-like precipitate grows thicker, some dissolution continues to occur, although it becomes more difficult as a result of the ion diffusion through the newly formed HA-like phase, and into the surrounding medium.

An ATR–FTIR analysis of the new precipitate layer was performed to confirmed the apatite type growing over the scaffold (Fig. 7). It could be observed absorptions corresponding to phosphate and silicate groups (overlapped in 1016, 942 and 869 cm^{-1}), and phosphate groups in 601, 548 cm^{-1}. In addition, infrared spectra showed bands related to the presence of OH^- groups centered at 3396 cm^{-1} and 1638 cm^{-1}, and as

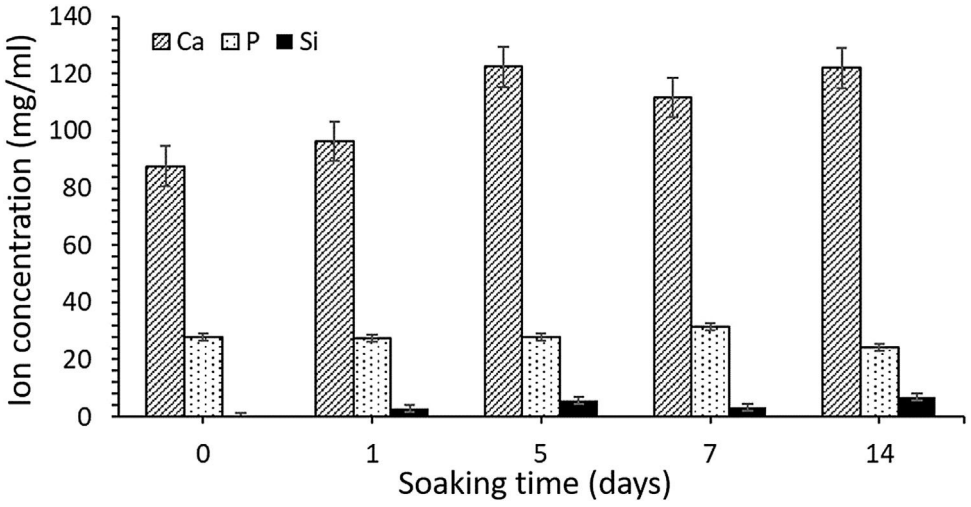

Fig. 6 – ICP-OES analysis for changes in SBF ion concentration, after different soaking times.

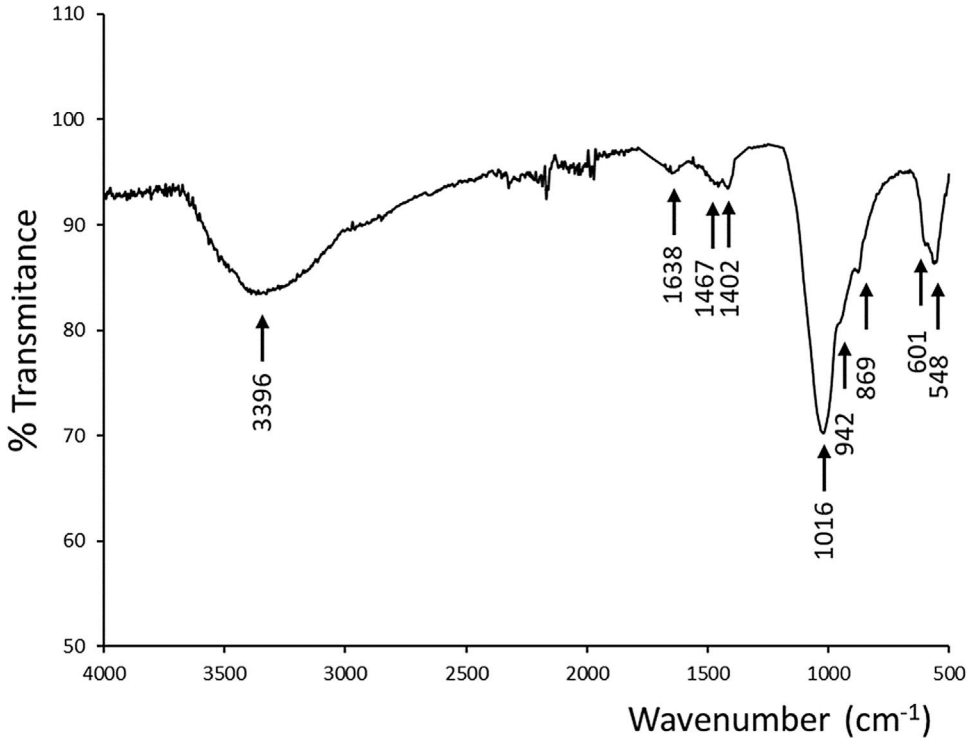

Fig. 7 – ATR–FTIR spectra from the precipitate layer of the 14 days SBF soaked scaffold.

well bands corresponding to CO_3^{2-} groups at 1467 cm^{-1} and 1402 cm^{-1}, confirming the presence of CHA because of the partial substitution of the phosphate groups in the HA-like crystalline structure [24].

One of the main properties of biomaterials in order to be biocompatible is their effect in cells proliferation. Therefore, the effect of uncoated and coated samples in ahMSCs proliferation was assessed by culturing ahMSCs on $SiCaP_2O_5$ ceramic and rGO-$SiCaP_2O_5$ scaffold for 7 days. Interestingly, the cells cultured on both samples showed a rate of proliferation greater compared to the control ($p < 0.05$) (Fig. 8a). However, there was no significant changes observed associated to the reduced graphene coating.

The cytotoxic results (Fig. 8b) showed that the cells cultured on ceramic $SiCaP_2O_5$ and rGO-$SiCaP_2O_5$ scaffold had significantly higher OD value at 570 nm compared to control ($p < 0.05$). Reduced graphene coated scaffold had slightly higher OD value, however, the differences were insignificant. Interestingly, the cells cultured on studied samples had 2 folds higher rate of compatibility compared to control cells, which is in agreement with the cell proliferation study (Fig. 8a).

The cell loading ability was determined by seeding ahMSCs with a cell density of 1×10^5 cells per sample (Fig. 9). After 6 h of incubation, the capacity of uncoated and coated samples was in general lower than control group (cells without ceramic in 2D culture), however the difference was insignificant. Loading

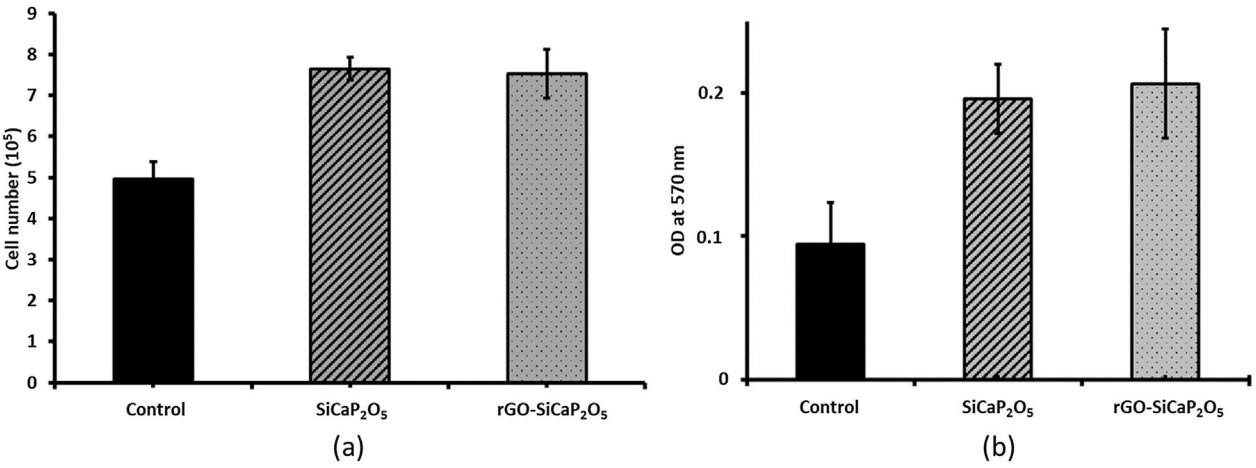

Fig. 8 – (a) Proliferation cells on $SiCaP_2O_5$ ceramic and $rGO\text{-}SiCaP_2O_5$ scaffold, and (b) Cytotoxicity study for $SiCaP_2O_5$ ceramic and $rGO\text{-}SiCaP_2O_5$ scaffold.

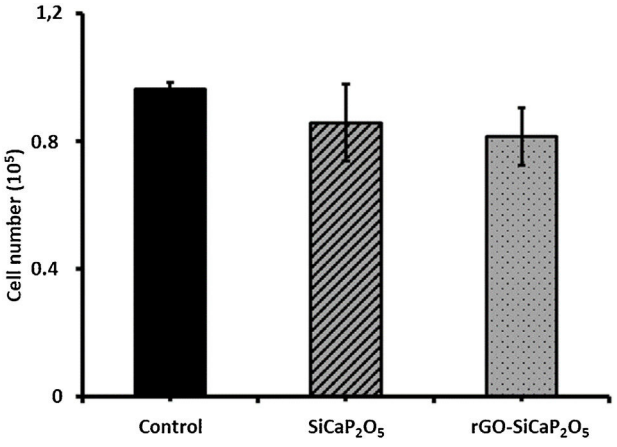

Fig. 9 – Cell loading ability for $SiCaP_2O_5$ ceramic and $rGO\text{-}SiCaP_2O_5$ scaffold.

capacity of ahMSCs was lower in $rGO\text{-}SiCaP_2O_5$ scaffold from $SiCaP_2O_5$ ceramic.

The cell adhesion behavior of ahMSCs on uncoated and coated samples was determined on 3 and 7 days by SEM analysis of surface's morphology (Fig. 10). In general, it had good ahMSCs adhesion, and cells were grown with more interconnected filaments penetrated in many directions. As expected, the number of cells spreading was higher in day 7 compared to day 3 and more in $rGO\text{-}SiCaP_2O_5$ scaffold than $SiCaP_2O_5$ ceramic. Interestingly, the surface of rGO coated scaffold was completed covered by ahMSCs with more flat-shape cells through filament-like interconnection throughout surface, which directly claimed the biocompatibility of rGO coated $SiCaP_2O_5$ scaffold for culturing ahMSCs.

Discussion

In the last decades the search of an appropriate scaffold for tissue engineering has focused a lot of attention. For this aim, bioceramics such as calcium phosphate have shown good properties due to their mineralogical structure close to the natural bone, even more when they include ions such as silicon in their composition [25,26]. Nurse's A phase ($SiCaP_2O_5$ ceramic) has shown to be an excellent scaffold for tissue repair by studies developed in our laboratory [27], although it would be possible to improve their mechanical strength and osteoconductivity.

Graphene derivatives interactions with living organisms for regenerative medicine, have been extensively research, focusing specially on GO and rGO, confirming their biocompatibility [28–31]. Their unique two-dimensional structure and biological interface behavior [32], together with their excellent osteogenesis inducing capability, make GO and rGO highly promising materials for use as scaffolds in bone tissue engineering, collaborating with biomaterials such as HA, calcium silicate, chitosan and 45S5Bioglass® between others [33–37].

In order to improve biological properties in this study $SiCaP_2O_5$ ceramic was uniformly coated with reduced graphene oxide as a way to supplying large surface area, high reactivity and biocompatibility [12,38]. The reduction of GO to rGO removes partially oxygen-containing functional groups and restores the sp2 structure, resulting in an increase in conductivity [39]. This improved conductivity is beneficial for the creation of a suitable signal conduction between cells and scaffolds, which is important for many tissue engineering applications [40].

Solid-state reaction was used to prepare the starting ceramic material, that was then uniformly coated with rGO. Mineralogical characterization of coated and uncoated samples by XRD (Fig. 1) indicated a monophasic composition concordant with the phase diagram Ca_2SiO_4—$Ca_3(PO_4)_2$ [41], corresponding to a solid solution of Nurse's A phase ($SiCaP_2O_5$), checked by the JCPDS data base. Any significant differences in diffraction peaks were observed after coating ($rGO\text{-}SiCaP_2O_5$).

In order to describe the elemental composition of scaffold, XPS analysis was realized from rGO surface and $SiCaP_2O_5$ ceramic (Fig. 2). As expected rGO surface present small quantities of calcium, silicon and phosphorous, that are present

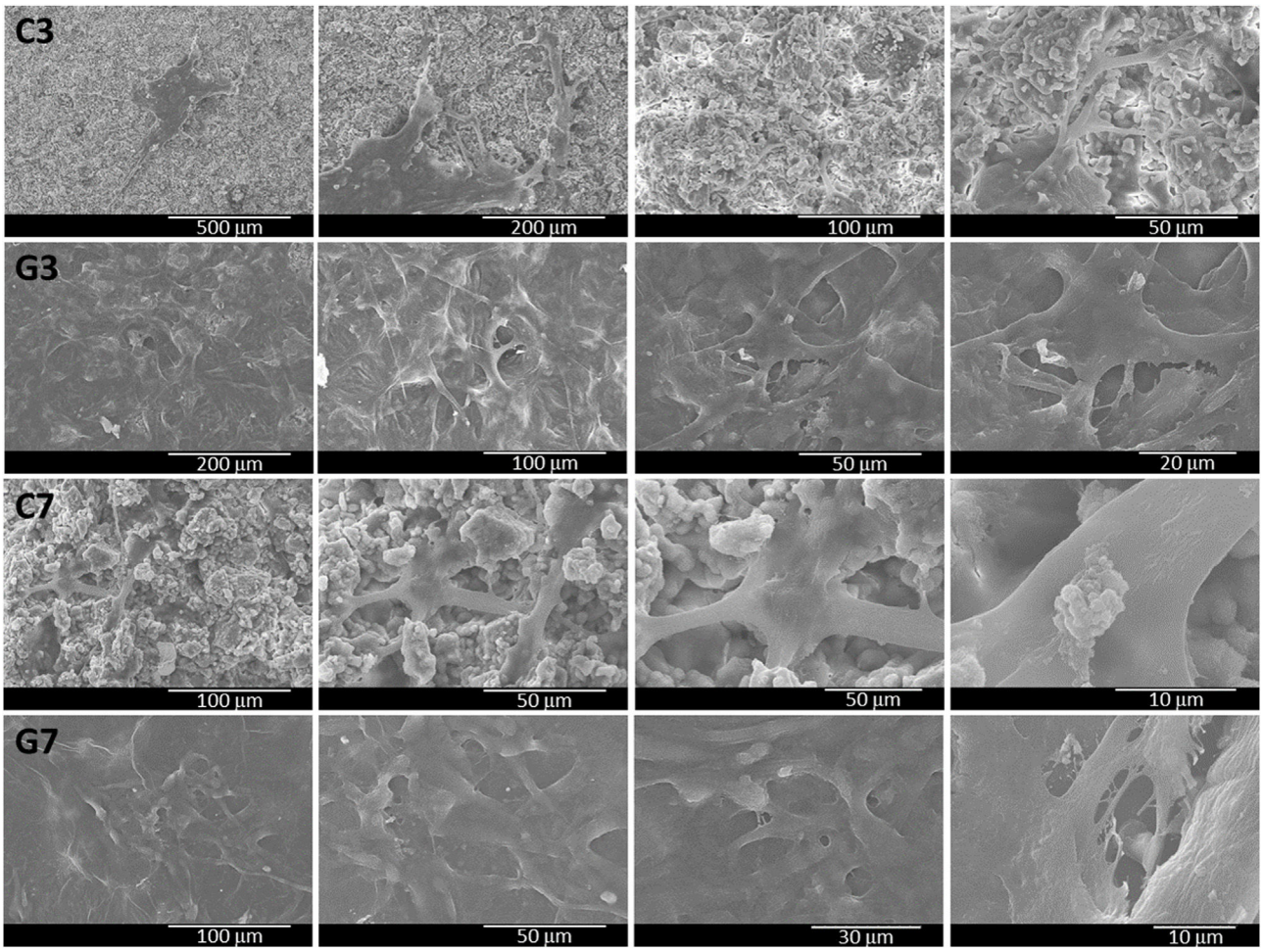

Fig. 10 – Cell morphological characteristics of ahMSCs cultured on bioactive ceramics for 3 and 7 days for C: $SiCaP_2O_5$ and G: rGO-coated $SiCaP_2O_5$.

in the ceramic structure below the coating. A bigger quantitative percentage of carbon (C1s) is observed in rGO coating, up to 97.09% (Table 1). The presence of rGO coating was confirmed by the deconvolution bands concerning to C═C sp2 and C—C sp3 hybridation, and also two deconvolution bands corresponding to hydroxyl groups C—OH and carboxylate groups O—C═O, according to literature [30,42].

Morphological analysis of the rGO-$SiCaP_2O_5$ scaffold was realized by SEM (Fig. 3). It showed a uniform and continuous coating of the $SiCaP_2O_5$ ceramic disk with a sheet of rGO, presenting a clear gap between the granular ceramic structure and the rGO sheet. The rough and undulating surface of rGO can provide physical stimulation that promotes cell adhesion, proliferation, and differentiation. The high surface area of rGO also provides more binding sites for osteoinductive factors, which can enhance osteogenic differentiation of the cells. Additionally, the π–π stacking and hydrogen bonding interactions of rGO can facilitate the adsorption and release of osteoinductive factors by non-covalent binding, further promoting osteogenesis [43].

Mercury porosimetry is a technique used to determine the pore structure of porous materials by measuring the penetration of mercury into the pores under increasing pressure. By analyzing the data, one can obtain information about the pore size distribution, porosity, and specific surface area of the material. In the case of this study, it was used to compare the microporosity of the coated and uncoated ceramic samples. Minor difference were observed for both samples, that presents two main absorptions in a similar way between 186 and 2 µm, slightly lower for rGO-$SiCaP_2O_5$ (continuous line in Fig. 4a). These absorptions correspond to intense peaks in the differential volume centered between 8 and 2 µm (Fig. 4b). The initial absorptions observed can be attributed to the filling of interparticle gaps, whereas the subsequent ones are likely caused by the filling of intraparticle voids. According to literature pore structures, because of the presence of larger surface areas, play a crucial role in enhancing the interaction between implanted material and natural bone, which can lead to an increase in protein absorption, ion exchange and bone-like apatite formation [44]. Any significant difference in porosity and density measures were found for uncoated and coated ceramic (Table 2), but a bigger intraparticle porosity was observed for rGO-$SiCaP_2O_5$ scaffold (16.48%) while it was 11.43% for uncoated ceramic. However, according to literature a surface increment and biocompatibility is expected due to rGO coating.

Scaffold's bioactivity was studied in vitro according to Standard ISO/FDIS 23317:2014 [21], reflecting the ability to stimulate calcium phosphate precipitate formation through immersion in SBF for 1, 5 and 7 days (Fig. 5a–c). After 1 day soaking no indication of bioactivity was found on the scaffold's surface, but it appeared at 5 days, when some isolated spheres and some groups of them were found on the surface. The surface appeared completely covered with a precipitate layer after 7 days of soaking in SBF, appearing even some cracking because of the vacuum used by SEM analysis. Extending the time of immersion in SBF until 14 days and realizing cross-section analysis (Fig. 5d), a uniform and continuous precipitate layer was observed above the rGO coating sheet, reaching thickness of 8.6 μm. Results obtained for this potential scaffold presents no significate differences in bioactivity rate and grade from $SiCaP_2O_5$ ceramic, previously studied in our laboratory [23].

The concentrations of silicon, calcium and phosphorus ion released were measured using ICP-OES after different immersion times in SBF (Fig. 6). Initial composition of SBF is included in results as 0 days soaking time. It was observed an increment in Ca and Si ion concentration until day 5 of soaking, which it is correlated with an initial dissolution of the ceramic prior to reaction with serum. After that time dissolution seems to be present at the same time HA-like precipitate layer is growing on the surface of scaffold, what difficult the ion diffusion processes across these layer.

Chemical composition of new precipitate layer, with a Ca/P ratio of 2.6 measured by EDS, was analyzed by ATR–FTIR (Fig. 7). In addition to absorptions corresponding to phosphate and silicate groups by means of serum used in bioactivity assay, absorption bands of hydroxyl and carbonate groups led us to confirm the presence of a CHA phase. This apatite deficient in calcium is partially substituted with silicon from the physiologic medium.

Scaffolds based on rGO have demonstrated their ability to promote cell proliferation and differentiation by enhancing cell-scaffold and cell-cell interactions through a variety of cellular signals, such as chemical or electrical signals [45]. This can be attributed to the unique properties of rGO, including its high surface area, excellent mechanical and electrical properties, high biocompatibility, and ability to promote cell adhesion and proliferation [46–50]. Additionally, the tunable properties of scaffolds incorporating rGO offers advantages such as improving hydrophilicity, mechanical strength, protein adsorption and stability, cell adhesion, proliferation, and enhancing electrical properties of the scaffolds [51–54]. These properties make them potentially useful in tissue engineering and regenerative medicine applications, providing an optimal environment for cells to adhere and proliferate [55].

The in vitro cell culture study confirmed that the $SiCaP_2O_5$ ceramic and rGO-$SiCaP_2O_5$ scaffold increased the ahMSCs proliferation rate than control (Fig. 8a), which ultimately proved the efficiency of these samples on tissue engineering application. It is well known that the biomaterials which stimulate the proliferation rate of biological cells directly claim the biocompatibility in practical application. The present study results of in vitro cell cultures were in total agreement with literature [56–59].

Furthermore, rGO has shown a higher capability in electron transferring which may be effective in accelerating differentiation [60], specially adipogenesis and osteogenesis through an improvement in the adsorption of differentiation factors and cell adhesion [61], and it is suggested as more compatible [62–64]. As well, some studies have suggested that rGO may induce the production of reactive oxygen species and activate specific signaling pathways that promote angiogenesis [65].

There are studies that have been shown cytotoxicity when rGO is used, because of some variation in physical properties derived from the method of synthesis. Regarding cytotoxicity, it could be influence for dose, surface charge or lateral size [66,67], however, in this study any sign of cytotoxicity was found (Fig. 8b).

Regarding to cell loading ability (Fig. 9), ahMSCs loading capacity of rGO-$SiCaP_2O_5$ was slightly lower than $SiCaP_2O_5$ one.

The morphological changes of ahMSCs seeded on bioactive samples after 3 and 7 days were determined by SEM (Fig. 10). It was observed adhesion and growing for cells with interconnected filaments extending over the surface. It is worth mentioning that rGO-$SiCaP_2O_5$ scaffold appeared completely cover of cells after 7 days what confirmed a better environment for growing and proliferation cells expected after rGO coating.

Another advantage reported for scaffolds' rGO incorporation is the excellent mechanical properties [68–70]. Mechanical properties will be presented in further studies.

Conclusion

The developed scaffold combines a calcium silicophosphate ceramic that provide a mineralogical composition similar to natural bone, with an rGO coating. Although both have proven their excellent in vitro bioactivity, rGO-$SiCaP_2O_5$ scaffold has shown an increasing osteoconductivity capability by inherent π–π conjugation, with any toxic effect in ahMSCs. The compatibility of the scaffold has been proved with good cell adherent properties, which would allow its use as potential scaffold for application in the future bone regenerative medicine

Acknowledgments

This work is part of the project PID2020-116693RB-C21 and PID2020-116693RB-C22, funded by MCIN/AEI/10.13039/501100011033 Spain. Grant CIAICO/2021/157 funded by Generalitat Valenciana Spain.

REFERENCES

[1] J. Li, H. Zeng, Z. Zeng, Y. Zeng, T. Xie, Promising graphene-based nanomaterials and their biomedical applications and potential risks: a comprehensive review, ACS Biomater. Sci. Eng. 7 (2021) 5363–5396, http://dx.doi.org/10.1021/acsbiomaterials.1c00875.
[2] A. Díaz-Arca, P. Velasquez, P. Mazón, P.N. De Aza, Mechanism of in vitro reaction of a new scaffold ceramic similar to porous bone, J. Eur. Ceram. Soc. 40 (2020) 2200–2206, http://dx.doi.org/10.1016/j.jeurceramsoc.2020.01.045.
[3] A. Díaz-Arca, P. Ros-Tárraga, M.J. Martínez, A.H. De Aza, L. Meseguer-Olmo, P. Mazón, et al., Micro-/nano-structured

ceramic scaffolds that mimic natural cancellous bone, Materials 14 (2021) 1–17, http://dx.doi.org/10.3390/ma14061439, 1439.
[4] K. Kenry, W.C. Lee, K.P. Loh, C.T. Lim, When stem cells meet graphene: opportunities and challenges in regenerative medicine, Biomaterials 155 (2018) 236–250, http://dx.doi.org/10.1016/j.biomaterials.2017.10.004.
[5] Q. Zhang, Z. Wu, N. Li, Y. Pu, B. Wang, T. Zhang, et al., Advanced review of graphene-based nanomaterials in drug delivery systems: synthesis, modification, toxicity and application, Mat. Sci. Eng. C 77 (2017) 1363–1375, http://dx.doi.org/10.1016/j.msec.2017.03.196.
[6] C. Gao, T. Liu, C. Shuai, S. Peng, Enhancement mechanisms of graphene in nano-58S bioactive glass scaffold: mechanical and biological performance, Sci. Rep. 4 (2015) 04712, http://dx.doi.org/10.1038/srep04712.
[7] S.Y. Park, J. Park, S.H. Sim, M.G. Sung, K.S. Kim, B.H. Hong, et al., Enhanced differentiation of human neural stem cells into neurons on graphene, Adv. Mater. 23 (2011) H263, http://dx.doi.org/10.1002/adma.201101503.
[8] X. Shi, H. Chang, S. Chen, C. Lai, A. Khademhosseini, H. Wu, Regulating cellular behaviour on few-layer reduced graphene oxide films with well-controlled reduction states, Adv. Funct. Mater. 22 (2012) 751–759, http://dx.doi.org/10.1002/adfm.201102305.
[9] S. Kim, S.H. Ku, S.Y. Lim, J.H. Kim, C.B. Park, Graphene-biomineral hybrid materials, Adv. Mater. 23 (2011) 2009–2014, http://dx.doi.org/10.1002/adma.201100010.
[10] S. Pei, H.M. Cheng, The reduction of graphene oxide, Carbon N. Y. 50 (2012) 3210–3228, http://dx.doi.org/10.1016/j.carbon.2011.11.010.
[11] R. Tarcan, O. Todor-Boer, I. Petrovai, C. Leordean, S. Astilean, I. Botiz, Reduced graphene oxide today, J. Mater. Chem. C 8 (2020) 1198–1224, http://dx.doi.org/10.1039/C9TC04916A.
[12] D. Báez, H. Pardo, I. Laborda, J. Marco, C. Yáñez, S. Bollo, Reduced graphene oxides: influence of the reduction method on the electrocatalytic effect towards nucleic acid oxidation, Nanomaterials 7 (2017) 168, http://dx.doi.org/10.3390/nano7070168.
[13] S. Stankovich, D.A. Dikin, R.D. Piner, K.A. Kohlhaas, A. Kleinhammes, Y. Jia, et al., Synthesis of graphene-based nanosheets via chemical reduction of exfoliated graphite oxide, Carbon N. Y. 45 (2007) 1558–1565, http://dx.doi.org/10.1016/j.carbon.2007.02.034.
[14] S. Lv, Y. Ma, C. Qiu, T. Sun, J. Liu, Q. Zhou, Effect of graphene oxide nanosheets of microstructure and mechanical properties of cement composites, Construct. Build. Mater. 49 (2013) 121–127, http://dx.doi.org/10.1016/j.conbuildmat.2013.08.022.
[15] S. Sharma, N.C. Kothiyal, Influence of graphene oxide as dispersed phase in cement mortar matrix in defining the crystal patterns of cement hydrates and its effect on mechanical, microstructural and crystallization properties, RSC Adv. 5 (2015) 52642–52657, http://dx.doi.org/10.1039/C5RA08078A.
[16] L. Meseguer-Olmo, S. Aznar-Cervantes, P. Mazón, P.N. De Aza, "In vitro" behaviour of adult mesenchymal stem cells of human bone marrow origin seeded on a novel bioactive ceramics in the Ca_2SiO_4–$Ca_3(PO_4)_2$ system, J. Mater. Sci. Mater. Med. 23 (2012) 3003–3014, http://dx.doi.org/10.1007/s10856-012-4742-z.
[17] P. Mazón, D. García-Bernal, L. Meseguer-Olmo, F. Cragnolini, P.N. De Aza, Human mesenchymal stem cell viability, proliferation and differentiation potential in response to ceramic chemistry and surface roughness, Ceram. Int. 41 (2015) 6631–6644, http://dx.doi.org/10.1016/j.ceramint.2015.01.110.
[18] R. Rabadán-Ros, S. Aznar-Cervantes, P. Mazón, P. Ros-Tárraga, P.N. De Aza, L. Meseguer-Olmo, Nurse's A-phase material enhance adhesion, growth and differentiation of human bone marrow-derived stromal mesenchymal stem cells, Materials 10 (2017) 1–15, http://dx.doi.org/10.3390/ma10040347, 347.
[19] G.J. Lugo, P. Mazón, C. Baudín, P.N. De Aza, Nurse's A-phase: synthesis and characterization in the binary system Ca_2SiO_4–$Ca_3(PO_4)_2$, J. Am. Ceram. Soc. 98 (2015) 3042–3046, http://dx.doi.org/10.1111/jace.13747.
[20] M.J. Fernández-Merino, L. Guardia, J.L. Paredes, S. Villar-Rodil, P. Solís-Fernández, A. Martínez-Alonso, et al., Vitamin C is an ideal substitute for hydrazine in the reduction of graphene oxide suspensions, J. Phys. Chem. C 4 (2013) 6426–6432, http://dx.doi.org/10.1021/jp100603h.
[21] ISO/FDIS 23317, Implants for surgery. In vitro evaluation for apatite-forming ability of implant materials (2014).
[22] J. Elango, R. Bushin, A. Lijnev, P.N. De Aza, C. Pérez-Albacete, J.M. Granero, et al., The effect of germanium-loaded hydroxyapatite biomaterials on bone marrow mesenchymal stem cells growth, Cells 11 (2022) 1–21, http://dx.doi.org/10.3390/cells11192993, 2993.
[23] R. Rabadán-Ros, P. Mazón, S. Serena, M.A. Sainz, L. Meseguer-Olmo, P.N. De Aza, In vitro behaviour of nurse's ass-phase: a new calcium silicophosphate ceramic, J. Eur. Ceram. Soc. 37 (2017) 2943–2952, http://dx.doi.org/10.1016/j.jeurceramsoc.2017.03.014.
[24] F. Ren, Y. Ding, Y. Leng, Infrared spectroscopic characterization of carbonated apatite: a combined experimental and computational study, J. Biomed. Mater. Res. A 102 (2014) 496–505, http://dx.doi.org/10.1002/jbm.a.34720.
[25] R.G. Carrodeguas, S. De Aza, α-Tricalcium phosphate: synthesis, properties and biomedical applications, Acta Biomater. 7 (2011) 3536–3546, http://dx.doi.org/10.1016/j.actbio.2011.06.019.
[26] J. Lu, H. Yu, Ch. Chen, Biological properties of calcium phosphate materials for bone repair: a review, RSC Adv. 8 (2018) 2015–2033, http://dx.doi.org/10.1039/C7RA11278E.
[27] G.J. Lugo, P. Mazón, P.N. De Aza, Material processing of a new calcium silicophosphate ceramic, Ceram. Int. 42 (2016) 673–680, http://dx.doi.org/10.1016/j.ceramint.2015.08.164.
[28] M. Omidi, A. Fathinia, M. Farahani, Z. Niknam, A. Yadegari, M. Hashemi, Bio-Applications of Graphene Composites: From Bench to Clinic. Advanced 2D Materials, John Wiley & Sons, New York, 2016, pp. 433–471, http://dx.doi.org/10.1002/9781119242635.ch11.
[29] Q.-Z. Chen, S.E. Harding, N.N. Ali, Biomaterials in cardiac tissue engineering: ten years of research survey, Mater. Sci. Eng. R Rep. 59 (2008) 1–37, http://dx.doi.org/10.1016/j.mser.2007.08.001.
[30] J. Jagiełło, A. Chlanda, M. Baran, M. Gwiazda, L. Lipinska, Synthesis and characterization of graphene oxide and reduced graphene oxide composites with inorganic nanoparticles for biomedical applications, Nanomaterials 10 (2020) 1846, http://dx.doi.org/10.3390/nano10091846.
[31] A.M. Pinto, I.C. Gonçalves, F.D. Magalhães, Graphene-based materials biocompatibility: a review, Colloids Surf. B Biointerfaces 111 (2013) 188–202, http://dx.doi.org/10.1016/j.colsurfb.2013.05.022.
[32] M. Adeel, M. Bilal, T. Rasheed, A. Sharma, H. Iqbal, Graphene and graphene oxide: functionalization and nano-bio-catalytic system for enzyme immobilization and biotechnological perspective, Int. J. Biol. Macromol. 120 (2018) 1430–1440, doi:S0141813018331611.
[33] J.H. Lee, S.-M. Lee, Y.C. Shin, H.H. Park, S.W. Hong, Spontaneous osteodifferentiation of bone marrow-derived mesenchymal stem cells by hydroxyapatite covered with

graphene nanosheets, J. Biomater. Tissue Eng. 6 (2016) 818–825, http://dx.doi.org/10.1166/jbt.2016.1506.
[34] H. Fan, L. Wang, K. Zhao, N. Li, Z. Shi, Z. Ge, et al., Fabrication, mechanical properties and biocompatibility of graphene reinforced chitosan composites, Biomacromolecules 11 (2010) 2345–2351, http://dx.doi.org/10.1021/bm100470q.
[35] Y. Liu, J. Huang, H. Li, Synthesis of hydroxyapatite-reduced graphite oxide nanocomposites for biomedical applications: oriented nucleation and epitaxial growth of hydroxyapatite, J. Mat. Chem. B 1 (2013) 1826–1834, http://dx.doi.org/10.1039/C3TB00531C.
[36] M. Mehrali, E. Moghaddam, S.F.S. Shirazi, S. Baradaran, M. Mehrali, Synthesis, mechanical properties and in vitro biocompatibility with osteoblasts of calcium silicate-reduced graphene oxide composites, ACS Appl. Mater. Interfaces 6 (2014) 3947–3962, http://dx.doi.org/10.1021/am500845x.
[37] H. Porwal, S. Grasso, L. Cordero-Arias, C. Li, A. Boccaccini, M. Reece, Processing and bioactivity of 45S5 Bioglass®-graphene nanoplatelets composites, J. Mat. Sci. Mat. Med. 25 (2014) 1403–1413, http://dx.doi.org/10.1007/s10856-014-5172-x.
[38] X. Wang, G. Shi, An introduction to the chemistry of graphene, Phys. Chem. Chem. Phys. 17 (2015) 28484–28504, http://dx.doi.org/10.1039/C5CP05212B.
[39] Q. Zhang, X. Liu, H. Meng, S. Liu, C. Zhang, Reduction pathway-dependent cytotoxicity of reduced graphene oxide, Environ. Sci. Nano 5 (2018) 1361–1371, http://dx.doi.org/10.1039/C8EN00242H.
[40] L. Jiang, D. Chen, Z. Wang, Z. Zhang, Y. Xia, H. Xue, et al., Preparation of an electrically conductive graphene oxide/chitosan scaffold for cardiac tissue engineering, Appl. Biochem. Biotechnol. 188 (2019) 952–964, http://dx.doi.org/10.1007/s12010-019-02967-6.
[41] G.J. Lugo, P. Mazón, P.N. De Aza, Phase transitions in single phase Si—Ca—P-based ceramic under thermal treatment, J. Eur. Ceram. Soc. 35 (2015) 3693–3700, http://dx.doi.org/10.1016/j.jeurceramsoc.2015.04.036.
[42] M.K. Rabchinskii, A.T. Dideikin, D.A. Kirilenko, M.V. Baidakova, V.V. Shnitov, F. Rotch, et al., Facile reduction of graphene oxide suspensions and films using glass wafers, Sci. Rep. 8 (2018) 1–11, http://dx.doi.org/10.1038/s41598-018-32488-x, 14154.
[43] W.C. Lee, C.H. Lim, H. Shi, L.A. Tang, Y. Wang, C.T. Lim, et al., Origin of enhanced stem cell growth and differentiation on graphene and graphene oxide, ACS Nano 5 (2011) 7334–7341, http://dx.doi.org/10.1021/nn202190c.
[44] J. Zhang, X. Luo, D. Barbieri, A.M.C. Barradas, J.D. De Bruijn, C.A. van Blitterswijk, et al., The size of surface microstructures as an osteogenic factor in calcium phosphate ceramics, Acta Biomater. 10 (2014) 3254–3263, http://dx.doi.org/10.1016/j.actbio.2014.03.021.
[45] R. Geetha, K. Muthoosamy, S. Manickam, A. Hilal-Alnaqbi, Graphene-based 3D scaffolds in tissue engineering: fabrication, applications, and future scope in liver tissue engineering, Int. J. Nanomed. 14 (2019) 5753–5783, http://dx.doi.org/10.2147/IJN.S192779.
[46] S. Agarwal, X. Zhou, F. Ye, Q. He, C.G.K. Chen, J. Soo, et al., Interfacing live cells with nanocarbon substrates, Langmuir 26 (2010) 2244–2247, http://dx.doi.org/10.1021/la9048743.
[47] S. Park, N. Mohanty, J.W. Suk, A. Nagaraja, J. An, R.D. Piner, et al., Biocompatible, robust free-standing paper composed of a TWEEN/graphene composite, Adv. Mater. Weinheim 22 (2010) 1736–1740, http://dx.doi.org/10.1002/adma.200903611.
[48] T.R. Nayak, H. Andersen, V.S. Makam, C. Khaw, S. Bae, X. Xu, et al., Graphene for controlled and accelerated osteogenic differentiation of human mesenchymal stem cells, ACS Nano 5 (2011) 4670–4678, http://dx.doi.org/10.1021/nn200500h.
[49] S. Ryoo, Y. Kim, M. Kim, D. Min, Behaviours of NIH-3T3 fibroblasts on graphene/carbon nanotubes: proliferation, focal adhesion, and gene transfection studies, ACS Nano 4 (2010) 6587–6598, http://dx.doi.org/10.1021/nn1018279.
[50] Y.C. Shin, J. Kim, S.E. Kim, S. Song, S.W. Hong, J. Oh, et al., RGD peptide and graphene oxide co-functionalized PLGA nanofiber scaffolds for vascular tissue engineering, Regen. Biomater. 4 (2017) 159–166, http://dx.doi.org/10.1093/rb/rbx001.
[51] S. Park, R.S. Ruoff, Chemical methods for the production of graphenes, Nat. Nanotech. 4 (2009) 217–224, http://dx.doi.org/10.1038/nnano.2009.58.
[52] E. Casero, A.M. Parra-Alfambra, M.D. Petit-Domínguez, F. Pariente, E. Lorenzo, C. Alonso, Differentiation between graphene oxide and reduced graphene by electrochemical impedance spectroscopy (EIS), Electrochem. Commun. 20 (2012) 63–66, http://dx.doi.org/10.1016/j.elecom.2012.04.002.
[53] J. Molina, J. Fernández, J.C. Inés, A.I. Del Río, J. Bonastre, F. Cases, Electrochemical characterization of reduced graphene oxide-coated polyester fabrics, Electrochim. Acta 93 (2013) 44–52, http://dx.doi.org/10.1016/j.electacta.2013.01.071.
[54] A. Rose, N. Raghavan, S. Thangavel, B. Uma-Maheswari, D.P. Nair, G. Venugopal, Investigation of cyclic voltammetry of graphene oxide/polyaniline/polyvinylidene fluoride nanofibers prepared via electrospinning, Mater. Sci. Semicond. Process. 31 (2015) 281–286, http://dx.doi.org/10.1016/j.mssp.2014.10.051.
[55] C. Fu, H. Bai, J. Zhu, Z. Niu, Y. Wang, J. Li, et al., Enhanced cell proliferation and osteogenic differentiation in electrospun PLGA/hydroxyapatite nanofiber scaffolds incorporated with graphene oxide, PLOS ONE 12 (2017) e0188352, http://dx.doi.org/10.1371/journal.pone.0188352.
[56] H. Elkhenany, L. Amelse, A. Lafont, S. Bourdo, M. Caldwell, N. Neilsen, et al., Graphene supports in vitro proliferation and osteogenic differentiation of goat adult mesenchymal stem cells: potential for bone tissue engineering, J. Appl. Toxicol. 35 (2015) 367–374, http://dx.doi.org/10.1002/jat.3024.
[57] N. Shadjou, M. Hasanzadeh, Graphene and its nanostructure derivatives for use in bone tissue engineering: recent advances, J. Biomed. Mater. Res. Part A 104A (2016) 1250–1275, http://dx.doi.org/10.1002/jbm.a.35645.
[58] H. Xie, T. Cao, F.J. Rodríguez-Lozano, E.K. Luong-Van, V. Rosa, Graphene for the development of the next generation of biocomposites for dental and medical applications, Dent. Mater. 33 (2017) 765–774, http://dx.doi.org/10.1016/j.dental.2017.04.008.
[59] L. Daneshmandi, M. Barajaa, A. Tahmasbi, S.A. Sydlik, C.T. Laurencin, Graphene-based biomaterials for bone regenerative engineering: a comprehensive review of the field and considerations regarding biocompatibility and biodegradation, Adv. Healthcare Mater. 10 (2021) 1–25, http://dx.doi.org/10.1002/adhm.202001414, 2001414.
[60] O. Akhavan, E. Ghaderi, E. Abouei, S. Hatamie, E. Ghasemi, Accelerated differentiation of neural stem cells into neurons on ginseng reduced graphene oxide sheets, Carbon N. Y. 66 (2014) 395–406, http://dx.doi.org/10.1016/J.CARBON.2013.09.015.
[61] S.R. Ignat, A.D. Lazar, A. Selaru, I. Samoila, G.M. Vlasceanu, M. Ionita, et al., Versatile biomaterial platform enriched with graphene oxide and carbon nanotubes for multiple tissue engineering applications, Int. J. Mol. Sci. 20 (2019) 1–19, http://dx.doi.org/10.3390/ijms20163868, 3868.
[62] M.C. Duch, G.R.S. Budinger, Y.T. Liang, S. Soberanes, D. Urich, Minimizing oxidation and stable nanoscale dispersion improves the biocompatibility of graphene in the lung, Nano Lett. 11 (2011) 5201–5207, http://dx.doi.org/10.1021/nl202515a.

[63] S.A. Sydlik, S. Jhunjhunwala, M.J. Webber, D.G. Anderson, R. Langer, In vivo compatibility of graphene oxide with differing oxidation states, ACS Nano 9 (2015) 3866–3874, http://dx.doi.org/10.1021/acsnano.5b01290.
[64] G. Zhao, H. Qing, G. Huang, G.M. Genin, T.J. Lu, Reduced graphene oxide functionalized nanofibrous silk fibroin matrices for engineering excitable tissues, NPG Asia Mater. 10 (2018) 982–994, http://dx.doi.org/10.1038/s41427-018-0092-8.
[65] S. Mukherjee, P. Sriram, A.K. Barui, S.K. Nethi, V. Veeriah, S. Chatterjee, et al., Graphene oxides show angiogenic properties, Adv. Healthc. Mat. 4 (2015) 1722–1732, http://dx.doi.org/10.1002/adhm.201500155.
[66] A. Jastrzębska, P. Kurtycz, A. Olszyna, Recent advances in graphene family materials toxicity investigations, J. Nanopart. Res. 14 (2012) 1–21, http://dx.doi.org/10.1007/s11051-012-1320-8.
[67] S.K. Misra, P. Kondaiah, S. Bhattacharya, C.N.R. Rao, Graphene as a nanocarrier for tamoxifen induces apoptosis in transformed cancer cell lines of different origins, Small 8 (2012) 131–143, http://dx.doi.org/10.1002/smll.201101640.
[68] K.S. Novoselov, V.I. Falko, L. Colombo, P.R. Gellert, M.G. Schwab, K. Kim, A roadmap for graphene, Nature 490 (2012) 192, http://dx.doi.org/10.1038/nature11458, 7419:.
[69] X. Huang, Z. Yin, S. Wu, X. Qi, Q. He, Q. Zhang, et al., Graphene-based materials: synthesis, characterization, properties, and applications, Small 7 (2011) 1876–1902, http://dx.doi.org/10.1002/smll.201002009.
[70] T. Kuila, S. Bose, P. Khanra, A.K. Mishra, N.H. Kim, J.H. Lee, Recent advances in graphene-based biosensors, Biosens. Bioelectron. 26 (2011) 4637–4648, http://dx.doi.org/10.1016/j.bios.2011.05.039.